

Facile synthesis of Ni₃S₂/rGO nanosheets composite on nickel foam as efficient electrocatalyst for hydrogen evolution reaction in alkaline media

Binhong He

College of Chemistry and Chemical Engineering, Hunan University, Changsha 410012, People's Republic of China; and School of Chemistry and Chemical Engineering, Hunan Institute of Science and Technology, Yueyang 414006, People's Republic of China

Minjie Zhou,^{a)} Zhaohui Hou, and Gangyong Li

School of Chemistry and Chemical Engineering, Hunan Institute of Science and Technology, Yueyang, People's Republic of China

Yafei Kuang^{b)}

College of Chemistry and Chemical Engineering, Hunan University, Changsha, People's Republic of China

(Received 29 April 2017; accepted 16 June 2017)

Three-dimensional Ni₃S₂-reduced graphene oxide (rGO) nanosheets composite is directly grown on nickel foam (Ni₃S₂-rGO@NF) by a one-step hydrothermal process involving *in situ* sulfurization of NF and reduction of GO. The introduction of GO is found not only to control the aggregation and the growth of Ni₃S₂ nanosheets, but also to increase the number of active sites and improve conductivity of composite. The heterogeneous Ni₃S₂-rGO@NF electrode as electrocatalysts for hydrogen evolution reaction (HER) exhibits significantly enhanced catalytic activity in alkaline media. The onset potential of Ni₃S₂-rGO@NF can be as low as ~0 mV, which is comparable to platinum, and only a small overpotential of ~44 mV is needed to reach a benchmark current density of 10 mA/cm². Moreover, it demonstrates a good stability. All evidences suggest that the *in situ* sulfurization can be considered as an effective way to prepare metal sulfides as electrocatalysts for hydrogen generation.

I. INTRODUCTION

Hydrogen production from electrocatalytic splitting of water to minimize global carbon emissions and to maintain sustainability is compelling.¹ To achieve this goal, highly active catalysts for the hydrogen evolution reaction (HER) are indispensable.² Noble metals, such as platinum (Pt), have been considered as one of state-of-the-art catalysts for HER in acidic medium because their free energy of hydrogen adsorption is approximately zero.^{3–5} Unfortunately, the high cost and scarcity seriously hinder its widespread application. It is imperative to design efficient kinds of HER catalyst that are made from earth-abundant elements. Indeed, tremendous efforts have been devoted in developing precious metal-free catalysts with high activity for HER over the past years.^{6–15} Among various materials, transition metal dichalcogenides (TMDs) have attracted increasing attention owing to their high catalytic activity.^{7–15} Experimental and theoretical studies showed that the HER performances

of TMDs were directly related to their composition,^{16–20} exposed active edge sites,^{4,7,9,21–23} and conductive substrates.^{7,24–30} Recently, various nanostructured Ni-based TMDs demonstrated impressive performances in HER.^{2,31,32} Particularly, Ni₃S₂ nanomaterial has been considered as one of the promising candidates for HER due to its low cost, high abundance, and easy preparation processing.^{33–38} Many studies showed that the electrocatalytic activities of three-dimensional (3D) Ni₃S₂ supported on Ni foam were higher than those of the molybdenum dichalcogenides in basic media because of their intrinsically high catalytic activity toward HER.^{35,36,39} Note that 3D structure can (i) facilitate the diffusion of electrolyte and hydrogen bubbles, (ii) ensure a large surface area associated with the nanostructured active materials along with the absence of binder, accelerating the surface reaction, and (iii) enable the direct contact of the nanostructured active materials to the underneath conductive substrate which ensures a possible high efficiency.^{40,41} However, to the best of our knowledge, little report has reported on the direct synthesis of 3D Ni₃S₂/graphene composite nanosheets on nickel foam (NF). Graphene displays extraordinary electronic conductivity, large specific surface area, and good chemical stability.⁴² The introduction of graphene is expected to

Contributing Editor: Xiaobo Chen

Address all correspondence to these authors.

^{a)}e-mail: zmj0104@126.com

^{b)}e-mail: yafeik@163.com

DOI: 10.1557/jmr.2017.270

improve the conductivity of the composites and facilitate the electron transfer, which is very important for high HER performance.^{7,37,43,44}

In this work, we present a facile method to synthesize 3D Ni₃S₂-rGO (reduced graphene oxide) nanosheets composite on NF. This composite shows outstanding HER catalytic ability. The effect of the rGO on the morphology, electrochemically active surface area (ECSA), and number of active sites of the Ni₃S₂ nanosheets were proposed. Compared to the Ni₃S₂@NF, the HER performance of the Ni₃S₂-rGO@NF composite is greatly improved with a near-zero onset potential.

II. EXPERIMENT SECTION

A. Materials

Natural graphite powder was purchased from Alfa Aesar, Tianjin, China (99.8%). Potassium permanganate (KMnO₄, 99%), hydrogen peroxide (H₂O₂, 30 wt%), concentrated sulfuric acid (H₂SO₄, 98 wt%), concentrated hydrochloric acid (HCl, 37 wt%), phosphorus pentoxide (P₂O₅, 98%), potassium persulfate (K₂S₂O₈, 99.5%), potassium hydroxide (KOH, 85%), acetone (CH₃COCH₃, 99%), and thiourea (NH₂CSNH₂, 99%) were purchased from Sinopharm Chemical Co., Ltd., Beijing, China. NF (99.95%) was purchased from Shengyuan Co., Ltd., Shanghai, China. The deionized (DI) water was prepared by the Millipore Milli-Q water purification system (18.2 MΩ; Millipore, Molsheim, France). All reagents were used as-received.

1. Synthesis of graphene oxide (GO)

GO was prepared by a modified Hummers method. A typical synthetic procedure can be divided into two steps. The first step is the preoxidation process. Briefly, 2.0 g of graphite was added to a mixture of 30 mL of concentrated H₂SO₄, 1 g of K₂S₂O₈, and 1 g of P₂O₅. The mixture was placed in an oil bath and continuously stirred at 80 °C for 6 h. The above mixture was diluted with 500 mL of DI water and then filtered through a 0.2 μm film and washed with DI water repeatedly until the pH is reached ~7. The filter cake was dried in an oven at 60 °C for 12 h. The second step is the oxidation process. 3 g of KMnO₄ was added gradually to 30 mL of concentrated H₂SO₄ in an ice water bath with stirring. 1 g of the pretreated graphite was added slowly to the mixture. The mixture was stirred at 20 °C for 1 h and then at 35 °C for 8 h before 50 mL of DI water was added to the mixture. After 15 min of stirring, the reaction was terminated by addition of 300 mL of DI water and 5 mL of H₂O₂ solution (30 wt%), and the mixture became bright yellow. Subsequently, the suspension was filtered, and rinsed with enough aqueous HCl (5 wt%) and then with a large amount of DI water until the pH reached ~7. Finally, the as-prepared GO hydrogel was dispersed in water under

ultrasonic treatment to form a homogeneous GO solution with a concentration of 8.8 mg/mL.

2. Synthesis of Ni₃S₂-rGO@NF composite

NF was pretreated by acetone, 3 M HCl and DI water, respectively, at room temperature for 10 min under ultrasonication. Typically, 0.8 g of thiourea was dispersed in 70 mL of GO solution (2.14 mg/mL) at room temperature with vigorous stirring for 30 min until a black homogeneous slurry was obtained. The mixture was then added into a Teflon lined stainless steel autoclave (100 mL) with a piece of the pretreated NF (1 × 1 cm). Hydrothermal reaction was carried out at 160 °C for 6 h. When the autoclave was cooled down to room temperature, the product was collected, washed with DI water and ethanol, and dried overnight in a vacuum oven at 60 °C. The resultant product was denoted as Ni₃S₂-rGO@NF. For comparison, Ni₃S₂@NF composite was prepared with the same procedures without GO.

B. Physical characterization

X-ray diffraction (XRD) patterns were recorded using a Rigaku smartlab X-ray diffractometer (Rigaku Corp, Tokyo, Japan) with Cu K_α radiation (λ = 0.15406 nm). Morphologies of the samples were characterized using scanning transmission electron microscopy (STEM; Tecnai G2 20 FEI Company, Eindhoven, Holland). The surface chemical composition and the atomic valence states were investigated by using X-ray photoelectron spectroscopy (XPS). XPS was performed under normal mode by using a Thermo Fisher Scientific Theta Probe Angle-resolved XPS system with monochromatic Al K_α X-ray (Thermo Fisher Scientific, Waltham, Massachusetts). The Raman Spectroscopy (Renishaw, London, U.K.) was also carried out with 514.5 nm excitation wave length.

C. Electrochemical characterization

All electrochemical measurements were performed in a three-electrode system at CHI660E electrochemical station (CH Instruments, Inc., Shanghai, China) using a saturated calomel electrode (SCE) and a Pt wire as the reference electrode and the counter electrode. The as-obtained samples were directly used as the working electrode. Electrochemical experiments were performed in 1 M KOH electrolyte. Linear sweep voltammetry (LSV) was conducted at a scan rate of 5 mV/s. Stability was examined by CV measurement for 1000 cycles at a scan rate of 50 mV/s in the potential range from -0.2 to 0.5 V versus SCE. The *I*-*t* curve and *V*-*t* curve were also recorded with a preset potential (50 mV versus RHE) and current density (15 mA/cm²), respectively. Impedance measurement was carried out in the frequency range from 0.01 Hz to 100 kHz with an amplitude potential of 5 mV.

Turnover frequency (TOF) was evaluated by CV tests in the electrolyte of phosphate buffered solution (pH = 7.0) at a scan rate of 50 mV/s in the potential range from -0.6 to 0.6 V versus SCE. The double layer capacitance (C_{dl}) was measured using a simple cyclic voltammetry method. The voltage window of cyclic voltammograms was -0.05 to 0.05 V versus SCE. The scan rates were 20, 40, 60, 80, 100, 120, 140, 160, 180, and 200 mV/s. C_{dl} was estimated by plotting the $\Delta j = (j_a - j_c)$ at 0.0 V versus SCE against the scan rate, where the slope was twice as the C_{dl} .

III. RESULTS AND DISCUSSION

Figure 1 shows the SEM images of the Ni₃S₂@NF and Ni₃S₂-rGO@NF. For comparison, bare NF presents a smooth surface as shown in Fig. S1. Figure 1(a) displays the SEM image of the Ni₃S₂@NF, showing that the NF is uniformly covered with interconnected Ni₃S₂ nanosheets. Figure 1(b) reveals that the introduction of rGO reduced the size of the Ni₃S₂ nanosheets. Moreover, the Ni₃S₂ nanosheets are anchored on rGO surface and interconnected to form the three-dimensional porous architecture. This result indicates that the Ni₃S₂ nanosheets have successfully fixed on the rGO.²⁹ The microstructure of the Ni₃S₂-rGO@NF composite was further examined by TEM [Fig. 1(c)]. The TEM image verifies that the ultrathin Ni₃S₂ nanosheets are homogeneously dispersed on the rGO sheets. HRTEM image shows that

the lattice spacing is 0.287 nm [Fig. 1(d)], which corresponds to the (110) plane of the rhombohedral Ni₃S₂ (JCPDS 44-1418).

Fig. 2 depicts the dark field image and energy-disperse spectroscopy (EDS) elemental mapping of Ni₃S₂-rGO@NF composite, which clearly shows that element Ni, S, and C distribute uniformly in the entire surface of the composite, suggesting the homogeneous growth of Ni₃S₂ on rGO sheets. The EDS result also indicates the existence of O in Ni₃S₂-rGO@NF composite, which could be mainly introduced by the rGO. To further acquire the structural information of the samples, XRD measurement was carried out. As shown in Fig. 3(a), the XRD peaks at $2\theta = 21.8, 31.1, 37.8, 49.7,$ and 55.1° are indexed to the (101), (110), (021), (211), and (122) planes of the rhombohedral Ni₃S₂ (JCPDS 44-1418), respectively.^{35,38} The diffraction peaks at $44.5, 51.8,$ and 76.4° are assigned to the (111), (200), and (220) planes of the cubic nickel (JCPDS 04-0850).^{34,35,38} Owing to the relatively low content of the rGO, only a very weak peak at $\sim 26^\circ$ corresponding to the (002) plane of rGO is observed. Raman spectroscopy was carried out to further characterize the as-synthesized Ni₃S₂/rGO composite. Fig. 3(b) exhibits a series of obvious peaks at 212, 301, and 348 cm^{-1} which are attributed to the vibration of Ni₃S₂.³⁴ The stretching motion of the sp^2 carbon atoms is assigned to the G-band at 1598 cm^{-1} . The D-band located at the 1350 cm^{-1} is attributed to defects and disorder in the graphene layers.⁴⁴ All these results

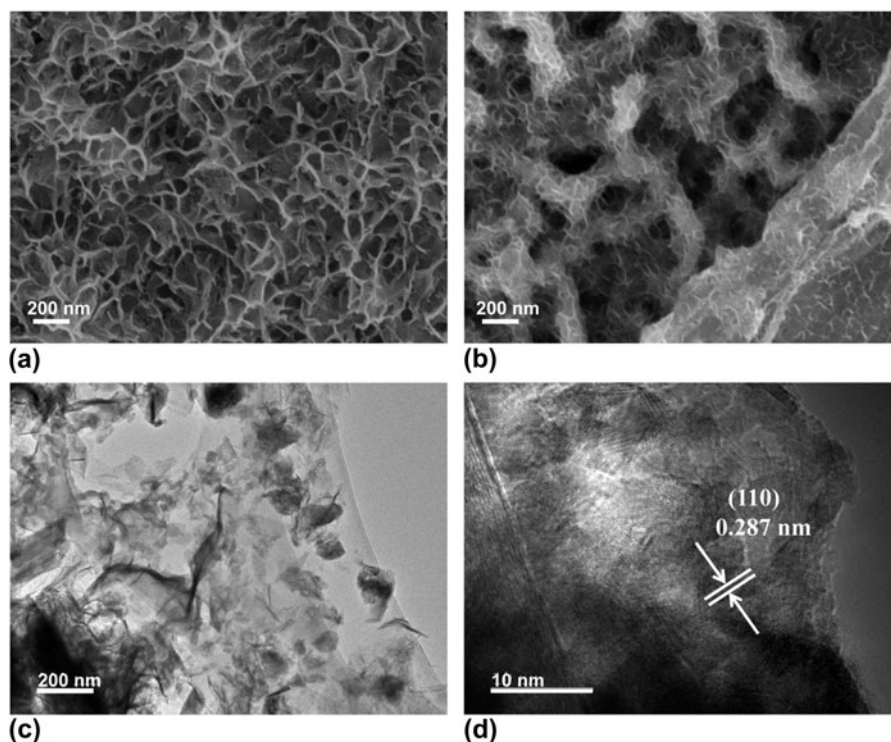
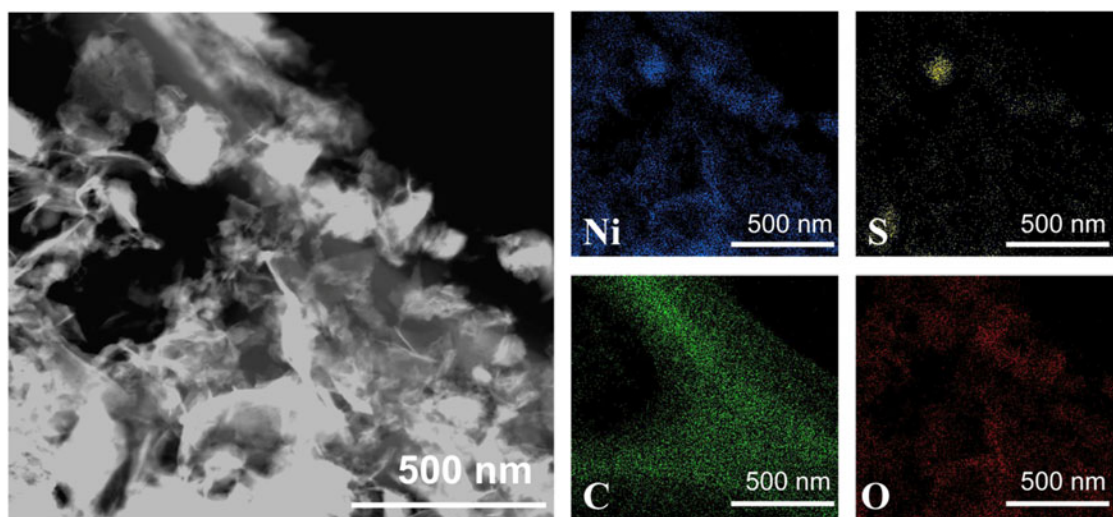
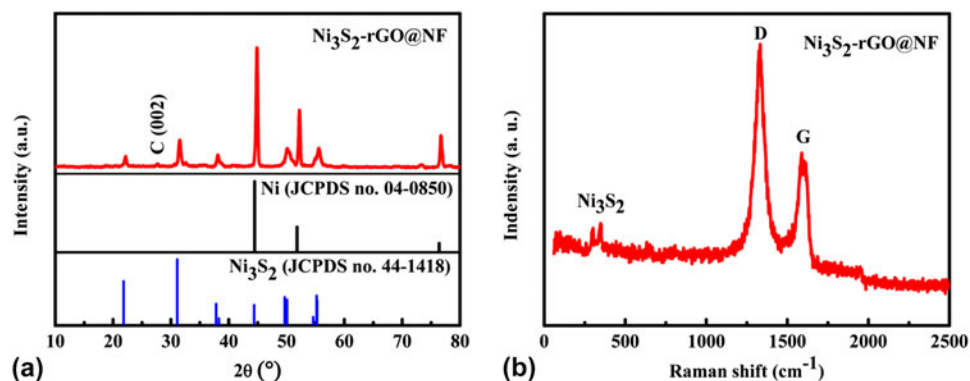


FIG. 1. SEM images of (a) Ni₃S₂@NF and (b) Ni₃S₂-rGO@NF. TEM (c) and HRTEM (d) images of Ni₃S₂-rGO@NF.

FIG. 2. Dark field image and elemental mapping of Ni₃S₂-rGO@NF.FIG. 3. XRD pattern (a) and Raman spectrum (b) of the Ni₃S₂-rGO@NF.

illustrate that 3D Ni₃S₂-rGO@NF was successfully prepared without other impurity.

The atomic valence states of the Ni₃S₂-rGO@NF composite were further studied by XPS analysis. The XPS survey spectrum [Fig. 4(a)] of the Ni₃S₂-rGO@NF composite displays an overview of the surface chemical composition, signaling the presence of Ni, S, C, and O. The high-resolution XPS spectrum of the Ni 2*p* could be fitted into four peaks [Fig. 4(b)]. Two main peaks located at 855.9 and 873.7 eV are attributed to Ni 2*p*_{3/2} and Ni 2*p*_{1/2}, respectively.⁴⁵ Figure 4(c) shows the high-resolution S 2*p* XPS spectrum. The two peaks centered at 163 and 164 eV correspond to the S 2*p*_{3/2} and S 2*p*_{1/2}, respectively.^{13,14} The high-resolution spectrum of O 1*s* can be deconvoluted into three peaks [Fig. 4(f)]: 531.2 eV (C=O), 532 eV (C–O–Ni), and 533.4 eV (C–O).^{46,47} Noting that the O 1*s* peak from the C–O–metal bond is located at 530–533 eV.⁴⁶ Therefore, the existence of C–O–Ni bond can be confirmed in the Ni₃S₂-rGO@NF composite.⁴⁷ The enhanced interfacial interaction between the rGO and Ni₃S₂ through the C–O–Ni bonding is

considered beneficial for enhancing the electron transport and structural stability of the Ni₃S₂/graphene electrode.⁴⁷ Figure 4(e) shows the deconvoluted C 1*s* XPS spectrum, where four different peaks are corresponding to C=C/C–C (284.8 eV), C–O (285.9 eV), C=O (287.3 eV), and O=C–O (288.8 eV) groups, respectively.⁴⁸ For comparison, Fig. 4(f) shows the fitted C 1*s* XPS spectrum of pure GO. Obviously, the intensities of the peaks from the C–O and C=O groups decrease dramatically, suggesting that the GO was reduced to form rGO during the hydrothermal treatment.²⁹

The catalytic performance of the Ni₃S₂-rGO@NF composite was investigated in 1.0 M KOH solution using a standard three-electrode system. For comparison, the commercial Pt/C, Ni₃S₂@NF composite, and bare Ni foam were also tested under identical conditions. Figure 5(a) shows the polarization curves in the potential window of 0.2 to –0.4 V versus RHE. The Ni₃S₂-rGO@NF composite shows significantly enhanced HER activity compared with the Ni₃S₂@NF composite. In sharp contrast, the bare Ni foam exhibits inferior HER activity. The

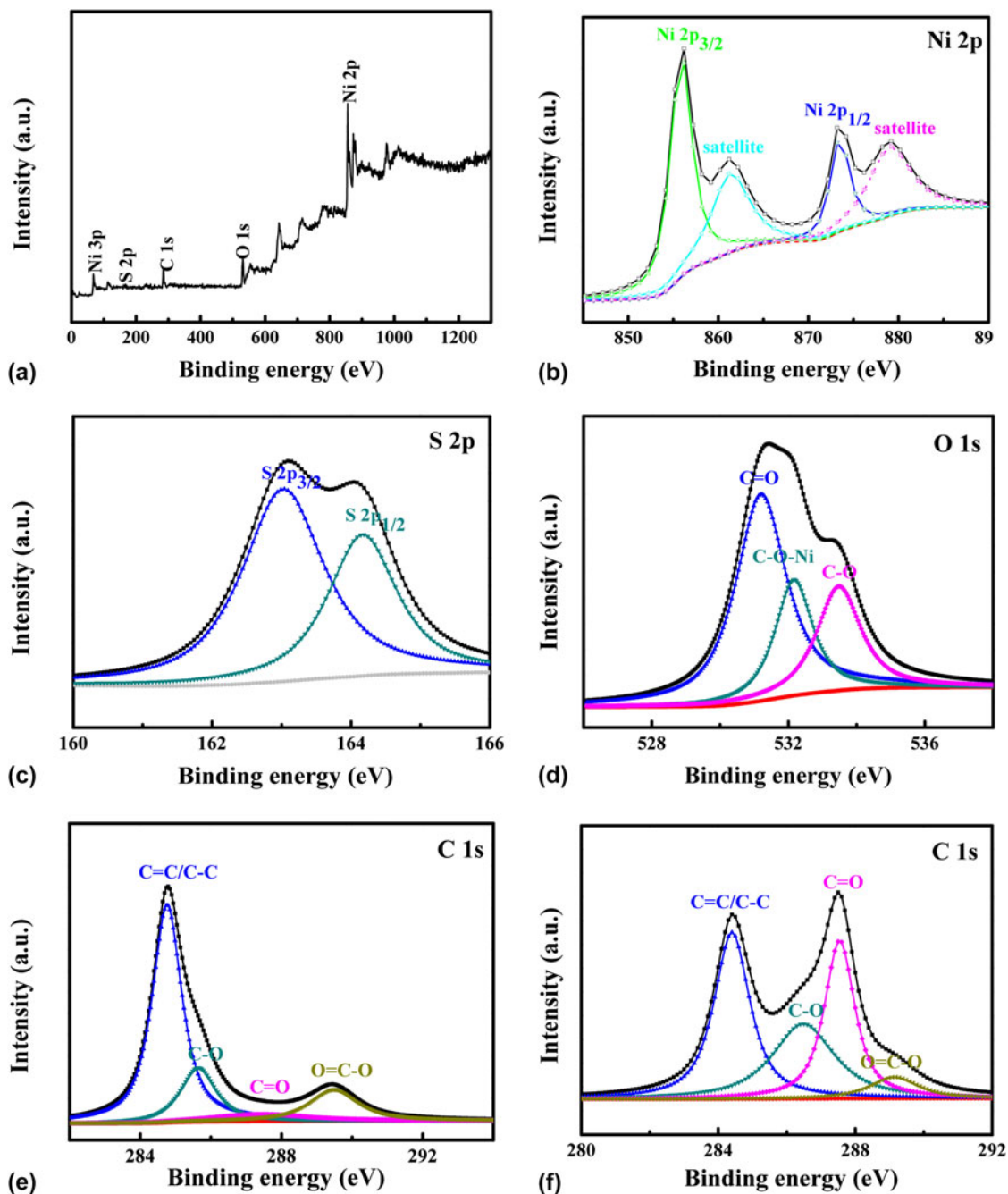


FIG. 4. (a) XPS survey spectrum. High-resolution (b) Ni 2p, (c) S 2p, (d) O 1s and (e) C 1s spectra of the Ni₃S₂-rGO@NF composite. (f) High-resolution C 1s spectrum of pure GO.

onset potential for the Ni₃S₂-rGO@NF composite is near 0 V versus RHE, which is comparable to that of the commercial Pt/C catalysts. The onset potentials of the Ni₃S₂@NF composite and Ni foam are 0.064 and 0.13 V versus RHE, respectively, confirming the superior HER activity of the Ni₃S₂-rGO@NF composite. Moreover, at a current density of 10 mA/cm², the overpotentials needed for the Ni₃S₂@NF composite and bare Ni foam are 161 and 243 mV, respectively. By contrast, the

Ni₃S₂-rGO@NF composite displays only a very low overpotential of ~44 mV. This is also superior to those of the other reported Ni₃S₂-based materials (Table I). These results reveal high catalytic activity of the Ni₃S₂-rGO@NF composite toward HER.

The Tafel plots, which are derived from the linear regions of the polarization curves, are shown in Fig. 5(b). The slope values for the bare Ni foam, Ni₃S₂@NF, Ni₃S₂-rGO@NF, and commercial Pt/C are 189, 115,

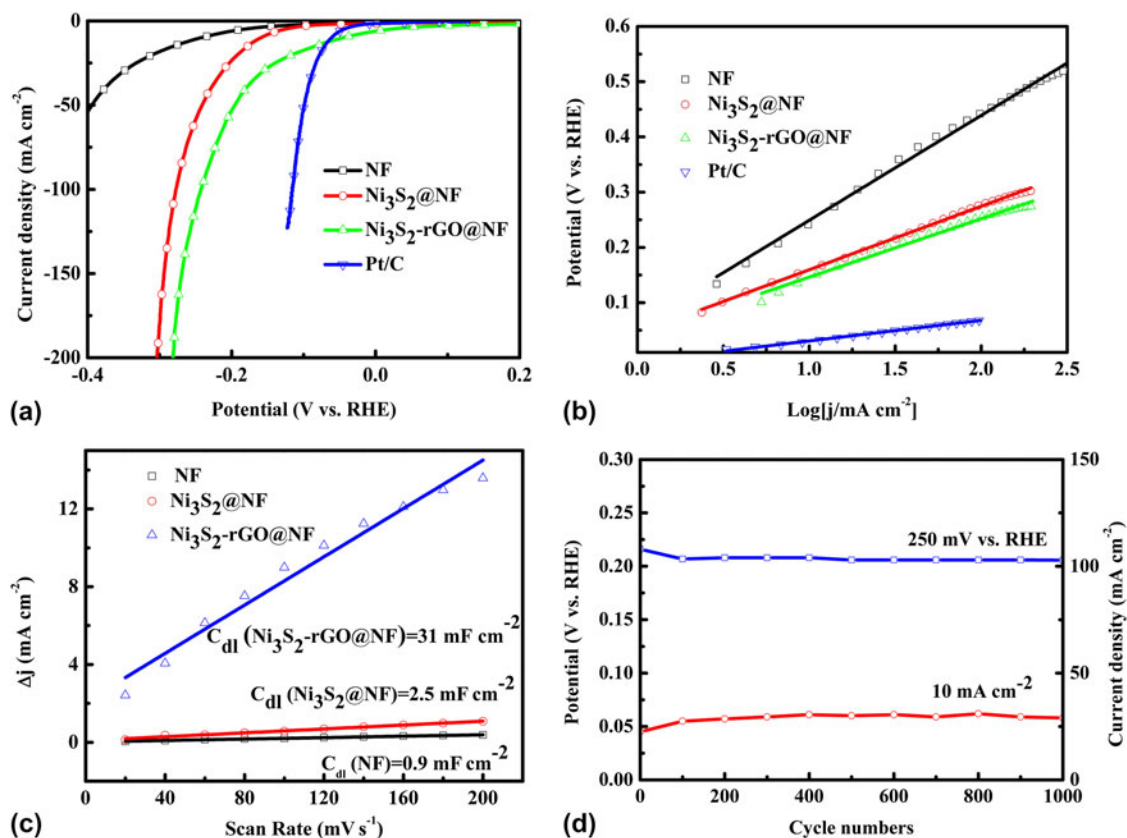


FIG. 5. Electrochemical measurements of various materials in 1 M KOH aqueous solution: (a) polarization curves, (b) Tafel plots (the dashed lines are the linear fitting results of corresponding Tafel curves), (c) charging current density difference ($\Delta j = j_a - j_c$) plotted against scan rate (the solid lines are the fitted results), and (d) stability test.

106, and 33 mV/dec, respectively. The Tafel slope of the Ni₃S₂-rGO@NF electrode is similar to that of the Ni₃S₂-based electrocatalysts reported in recent years (Table I). The Tafel slope is related to the mechanism of the HER process. In alkaline solutions, Tafel slope of 120, 40, or 30 mV/dec is expected if the Volmer ($\text{H}_2\text{O} + \text{e}^- \rightarrow \text{H}_{\text{ad}} + \text{OH}^-$), Heyrovsky ($\text{H}_2\text{O} + \text{H}_{\text{ad}} + \text{e}^- \rightarrow \text{H}_2 + \text{OH}^-$), or Tafel ($\text{H}_{\text{ad}} + \text{H}_{\text{ad}} \rightarrow \text{H}_2$) step is the rate-determining step, respectively.^{45,49} According to this, the Tafel slope of 106 mV/dec suggests a Volmer–Heyrovsky pathway on the surface of the Ni₃S₂-rGO@NF electrode.

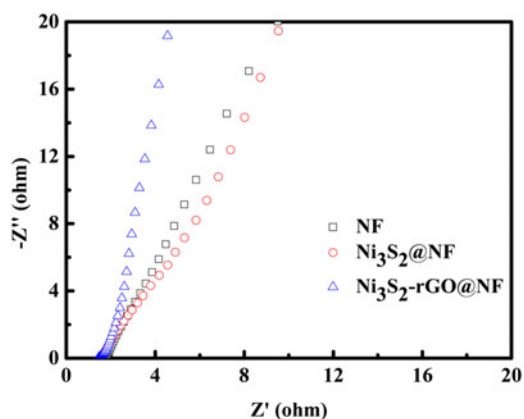
Obtaining the exact surface area was difficult due to the unknown capacitive behavior of the electrodes. However, the ECSA of the catalysts could be estimated from the C_{dl} based on CV tests (Fig. S2), as C_{dl} is linearly proportional to the effective active surface area. The linear slope of the capacitive current against scan rate was used to represent the ECSA. As can be seen from Fig. 5(c), the C_{dl} value of Ni₃S₂-rGO@NF composite is 31 mF/cm², much larger than that of in Ni₃S₂@NF (2.5 mF/cm²). By contrast, the Ni foam is only 0.9 mF/cm². This result suggests that the ECSA of the Ni₃S₂-rGO@NF electrode is much larger than that of the Ni₃S₂@NF electrode, and indicates more exposed active sites of the

Ni₃S₂-rGO@NF electrode.⁴⁵ Fig. S3 shows the voltammograms in the region of -0.6 to 0.6 V versus SCE at pH = 7. The integrated charge over the whole potential range should be proportional to the total number of active sites.⁴³ Assuming a one-electron process for both reduction and oxidation, the upper limit of the active sites could be calculated by the equation $n = Q/2F$, where Q is the number of voltammetric charges, F is Faraday constant, and n is the number of active sites. The calculated n values for the Ni₃S₂@NF and Ni₃S₂-rGO@NF electrodes are 1×10^{16} and 2.63×10^{17} cm⁻², respectively. This thus confirms the increased active sites for the Ni₃S₂-rGO@NF composite. The TOFs can be calculated according to the equations $\text{TOF} = I/2Fn$, where I is current during the LSV measurement.⁴³ The TOF values of the Ni₃S₂-rGO@NF and Ni₃S₂@NF electrodes were calculated to be 0.64 and 0.62 s⁻¹ at an overpotential of 200 mV at pH = 14 (Fig. S4). This also indicates the high HER activity of the Ni₃S₂-rGO@NF composite.⁴³

Electrocatalytic stability is another important criterion for the HER catalysts. The long-term stability of the Ni₃S₂-rGO@NF electrode was evaluated by CV test at a scan rate of 50 mV/s. As shown in Fig. 4(d) (the red

TABLE I. Comparison of key parameters of 3D Ni₃S₂-rGO@NF HER electrocatalyst.

Catalyst	Current density (<i>j</i> , mA/cm ²)	η at the corresponding <i>j</i> (mV)	Tafel slope (mV/dec)	Electrolyte	Ref.
Ni ₃ S ₂ /AT-Ni foam	10	200	107	1 M KOH	34
High-index faceted Ni ₃ S ₂ /NF	10	223	...	1 M KOH	35
Ni ₃ S ₂ /MWCNT-NC	1.2	400	167	1 M KOH	36
Ni ₃ S ₂ /Ni foam	13	500	167	1 M KOH	38
Ni ₃ S ₂ /Ni foam	10	123	110	1 M KOH	38
Ni ₃ S ₂ /Ni foam	10	232	106.4	1 M KOH	44
Ni ₃ S ₂ formed on nickel foam with rGO	10	157	92.8	1 M KOH	44
Ni ₂ P/Ti	20	138	60	1 M H ₂ SO ₄	2
NiSe/NF	10	96	120	1 M KOH	6
Metallic cobalt pyrite (CoS ₂)	10	145	51.6	0.5 M H ₂ SO ₄	14
V-doped Ni ₃ S ₂ nanowire	10	68	112	1 M KOH	15
1T-VS ₂ single crystalline nanosheets	10	68	34	0.5 M H ₂ SO ₄	18
MoS ₂ /graphene/Ni foam	10	>600	98	0.1 M KOH	19
Defect-rich MoS ₂	13	200	50	0.5 M H ₂ SO ₄	22
Molybdenum sulfide nanoparticles self-assembled on Au	10	>200	69	0.5 M H ₂ SO ₄	23
3D Ni ₃ S ₂ @NF	10	130	115	1 M KOH	This work
3D Ni ₃ S ₂ -rGO@NF	10	44	106	1 M KOH	This work

FIG. 6. Nyquist plots of the bare Ni foam, Ni₃S₂@NF and Ni₃S₂-rGO@NF electrodes.

curve), the overpotential required to maintain a current density of 10 mA/cm² increased by only 13 mV after 1000 cycles. Similarly, the current density at an overpotential of 250 mV is reduced by only 5 mA/cm² after 1000 cycles [the blue curve in Fig. 4(d)]. The *I-t* curve and *V-t* curve are also recorded in Fig. S5. After 10 h, only slight change of the current density or potential can be observed. All these evidences prove the high stability of the catalyst during HER. To further reveal the kinetics on the surface of the electrodes, Nyquist plots were obtained at the open-circuit voltage (Fig. 6). It can be seen that the electrolyte resistance and Warburg resistance of Ni₃S₂-rGO@NF is much lower. This is owed to the graphene that improves the conductivity of the composite. Hence, it can be concluded that the excellent HER activity of the Ni₃S₂-rGO@NF composite can be ascribed to the following reasons. On the one hand, the

introduction of rGO can increase the conductivity of the electrode. On the other hand, the confined growth of the Ni₃S₂ nanosheets could enlarge the surface area and provide more active sites.

IV. CONCLUSION

In summary, a facile one-pot hydrothermal synthesis method is developed to prepare the 3D Ni₃S₂-rGO@NF composite as electrocatalyst for HER. The introduction of rGO reduces the particle size of the Ni₃S₂, improves the conductivity of the catalyst, and increases the active sites toward HER. Because of these attributes, the 3D Ni₃S₂-rGO@NF electrode shows an extremely low onset potential (~0 V versus RHE). More importantly, the cathodic current increases sharply with potential, and a robust stability is demonstrated. Our findings show that the Ni₃S₂-rGO@NF composite can be a highly promising candidate electrocatalyst for electrochemical hydrogen generation.

ACKNOWLEDGMENTS

This work was supported by the National Natural Science Foundation of China (Grant No. 51372080) and the Research Foundation of Education Bureau of Hunan Province, China (Grant Nos. 16C0717 and 17K039).

REFERENCES

1. J.A. Turner: Sustainable hydrogen production. *Science* **305**(5686), 972 (2004).
2. Z.H. Pu, Q. Liu, C. Tang, A.M. Asiri, and X.P. Sun: Ni₂P nanoparticle films supported on a Ti plate as an efficient hydrogen evolution cathode. *Nanoscale* **6**(19), 11031 (2014).

- X.X. Zou and Y. Zhang: Noble metal-free hydrogen evolution catalysts for water splitting. *Chem. Soc. Rev.* **44**(15), 5148 (2015).
- X.D. Yan, L.H. Tian, K.X. Li, S. Atkins, H.F. Zhao, J. Murowchick, L. Liu, and X.B. Chen: FeNi₃/NiFeO_x nanohybrids as highly efficient bifunctional electrocatalysts for overall water splitting. *Adv. Mater. Interfaces* **3**(22), 1600368 (2016).
- J.K. Nørskov and C.H. Christensen: Toward efficient hydrogen production at surfaces. *Science* **312**(5778), 1322 (2006).
- C. Tang, N.Y. Cheng, Z.H. Pu, W. Xing, and X.P. Sun: NiSe nanowire film supported on nickel foam: An efficient and stable 3D bifunctional electrode for full water splitting. *Angew. Chem., Int. Ed.* **54**(32), 9351 (2015).
- T.F. Jaramillo, K.P. Jørgensen, J. Bonde, J.H. Nielse, and S. Hørch: Identification of active edge sites for electrochemical H₂ evolution from MoS₂ nanocatalysts. *Science* **317**(5834), 100 (2007).
- M.A. Lukowski, A.S. Daniel, F. Meng, A. Forticaux, L.S. Li, and S. Jin: Enhanced hydrogen evolution catalysis from chemically exfoliated metallic MoS₂ nanosheets. *J. Am. Chem. Soc.* **135**(28), 10274 (2013).
- D.S. Kong, H.T. Wang, J.J. Cha, M. Pasta, K.J. Koski, J. Yao, and Y. Cui: Synthesis of MoS₂ and MoSe₂ films with vertically aligned layers. *Nano Lett.* **13**(3), 1341 (2013).
- Z.Z. Wu, B.Z. Fang, A. Bonakdarpour, A.K. Sun, D.P. Wilkinson, and D.Z. Wang: WS₂ nanosheets as a highly efficient electrocatalyst for hydrogen evolution reaction. *Appl. Catal., B* **125**, 59 (2012).
- J. Lin, Z.W. Peng, G. Wang, D. Zakhidov, E. Larios, M.J. Yacaman, and J.M. Tour: Enhanced electrocatalysis for hydrogen evolution reactions from WS₂ nanoribbons. *Adv. Energy Mater.* **4**(10), 201301875 (2014).
- H.T. Wang, D.S. Kong, P. Johannes, J.J. Cha, G.Y. Zheng, K. Yan, N. Liu, and Y. Cui: MoSe₂ and WSe₂ nanofilms with vertically aligned molecular layers on curved and rough surfaces. *Nano Lett.* **13**(7), 3426 (2013).
- J. Zhang, S.H. Liu, H.W. Liang, R.H. Dong, and X.L. Feng: Hierarchical transition-metal dichalcogenide nanosheets for enhanced electrocatalytic hydrogen evolution. *Adv. Mater.* **27**(45), 7426 (2015).
- M.S. Faber, R. Dziejczak, M.A. Lukowski, N.S. Kaiser, Q. Ding, and S. Jin: High-performance electrocatalysis using metallic cobalt pyrite (CoS₂) micro- and nanostructures. *J. Am. Chem. Soc.* **136**(28), 10053 (2014).
- Y. Qu, M. Yang, J. Chai, Z. Tang, M. Shao, C.T. Kwok, M. Yang, Z. Wang, D. Chua, S. Wang, Z. Lu, and H. Pan: Facile synthesis of vanadium-doped Ni₃S₂ nanowire arrays as active electrocatalyst for hydrogen evolution reaction. *ACS Appl. Mater. Interfaces* **9**(7), 5959 (2017).
- Y. Jiao, Y. Zheng, M. Jaroniec, and S.Z. Qiao: Design of electrocatalysts for oxygen- and hydrogen-involving energy conversion reactions. *Chem. Soc. Rev.* **44**(8), 2060 (2015).
- C. Tang, L. Gan, R. Zhang, W. Lu, X. Jiang, A.M. Asiri, X. Sun, J. Wang, and L. Chen: Ternary Fe_xCo_{1-x}P nanowire array as a robust hydrogen evolution reaction electrocatalyst with Pt-like activity: Experimental and theoretical insight. *Nano Lett.* **16**(10), 6617 (2016).
- J. Yuan, J. Wu, W.J. Hardy, P. Loya, M. Lou, Y. Yang, S. Najmaei, M. Jiang, F. Qin, K. Keyshar, H. Ji, W. Gao, J. Bao, J. Kono, D. Natelson, P.M. Ajayan, and J. Lou: Facile synthesis of single crystal vanadium disulfide nanosheets by chemical vapor deposition for efficient hydrogen evolution reaction. *Adv. Mater.* **27**(37), 5605 (2015).
- X.M. Geng, W. Wu, N. Li, W.W. Sun, J. Armstrong, A. Al-hilo, M. Brozak, J.B. Cui, and T.P. Chen: Three-dimensional structures of MoS₂ nanosheets with ultrahigh hydrogen evolution reaction in water reduction. *Adv. Funct. Mater.* **24**(39), 6123 (2014).
- C. Tsai, F. Abild-Pedersen, and J.K. Nørskov: Tuning the MoS₂ edge-site activity for hydrogen evolution via support interactions. *Nano Lett.* **14**(3), 1381 (2014).
- J. Kibsgaard, Z.B. Chen, B.N. Reinecke, and T.F. Jaramillo: Engineering the surface structure of MoS₂ to preferentially expose active edge sites for electrocatalysis. *Nat. Mater.* **11**(11), 963 (2012).
- J. Xie, H. Zhang, S. Li, R. Wang, X. Sun, M. Zhou, J. Zhou, X.W. Lou, and Y. Xie: Defect-rich MoS₂ ultrathin nanosheets with additional active edge sites for enhanced electrocatalytic hydrogen evolution. *Adv. Mater.* **25**(40), 5807 (2013).
- T.Y. Wang, L. Liu, Z.W. Zhu, P. Papakonstantinou, J.B. Hu, H.Y. Liu, and M.X. Li: Enhanced electrocatalytic activity for hydrogen evolution reaction from self-assembled monodispersed molybdenum sulfide nanoparticles on an Au electrode. *Energy Environ. Sci.* **6**(2), 625 (2013).
- T.S. Hu, K. Bian, G.A. Tai, T. Zeng, X.F. Wang, X.H. Huang, K. Xiong, and K.J. Zhu: Oxidation-sulfidation approach for vertically growing MoS₂ nanofilms catalysts on molybdenum foils as efficient HER catalysts. *J. Phys. Chem. C* **120**(45), 25843 (2016).
- L. Liao, J. Zhu, X.J. Bian, L.N. Zhu, M.D. Scanlon, H.H. Girault, and B.H. Liu: MoS₂ formed on mesoporous graphene as a highly active catalyst for hydrogen evolution. *Adv. Funct. Mater.* **23**(42), 5326 (2013).
- Y.J. Chang, C.T. Lin, T.Y. Chen, C.L. Hsu, Y.H. Lee, W. Zhang, K.H. Wei, and L.J. Li: Highly efficient electrocatalytic hydrogen production by MoS_x grown on graphene-protected 3D Ni foams. *Adv. Mater.* **25**(5), 756 (2013).
- E.G.S. Firmiano, M.A.L. Cordeiro, A.C. Rabelo, C.J. Dalmaschio, A.N. Pinheiro, E.C. Pereira, and E.R. Leite: Graphene oxide as a highly selective substrate to synthesize a layered MoS₂ hybrid electrocatalyst. *Chem. Commun.* **48**(62), 7687 (2012).
- J. Guo, J. Wang, Z. Wu, W. Lei, J. Zhu, K. Xia, and D. Wang: Controllable synthesis of molybdenum-based electrocatalysts for a hydrogen evolution reaction. *J. Mater. Chem. A* **5**(2), 4879 (2017).
- X.L. Zheng, J.B. Xu, K.Y. Yan, H. Wang, Z.L. Wang, and S.H. Yang: Space-confined growth of MoS₂ nanosheets within graphite: The layered hybrid of MoS₂ and graphene as an active catalyst for hydrogen evolution reaction. *Chem. Mater.* **26**(7), 2344 (2014).
- C. Tang, L. Xie, X. Sun, A.M. Asiri, and Y. He: Highly efficient electrochemical hydrogen evolution based on nickel diselenide nanowall film. *Nanotechnology* **27**(20), 20LT02 (2016).
- P. Jiang, Q. Liu, and X. Sun: NiP₂ nanosheet arrays supported on carbon cloth: An efficient 3D hydrogen evolution cathode in both acidic and alkaline solutions. *Nanoscale* **6**(22), 13440 (2014).
- Y.Y. Wu, G.D. Li, Y.P. Liu, L. Yang, X.R. Lian, T. Asefa, and X.X. Zou: Overall water splitting catalyzed efficiently by and ultrathin nanosheet-built hollow Ni₃S₂-based electrocatalyst. *Adv. Funct. Mater.* **26**(27), 4839 (2016).
- G.F. Chen, T.Y. Ma, Z.Q. Liu, N. Li, Y.Z. Su, K. Davey, and S.Z. Qiao: Efficient and stable bifunctional electrocatalysts Ni/Ni_xM_y (M = P, S) for overall water splitting. *Adv. Funct. Mater.* **26**(19), 3314 (2016).
- C.B. Ouyang, X. Wang, C. Wang, X.X. Zhang, J.H. Wu, Z.L. Ma, S. Dou, and S.Y. Wang: Hierarchically porous Ni₃S₂ nanorod array foam as highly efficient electrocatalyst for hydrogen evolution reaction and oxygen evolution reaction. *Electrochim. Acta* **174**, 297 (2015).
- L.L. Feng, G.T. Yu, Y.Y. Wu, G.D. Li, H. Li, Y.H. Sun, T. Asefa, W. Chen, and X.X. Zou: High-index faceted Ni₃S₂ nanosheet

- arrays as highly active and ultrastable electrocatalysts for water splitting. *J. Am. Chem. Soc.* **137**(44), 14023 (2015).
36. T.W. Lin, C.J. Liu, and C.S. Dai: Ni₃S₂/carbon nanotube nanocomposite as electrode material for hydrogen evolution reaction in alkaline electrolyte and enzyme-free glucose detection. *Appl. Catal., B* **154–155**, 213 (2014).
37. N. Jiang, L. Bogoev, M. Popova, S. Gul, J. Yano, and Y.J. Sun: Electrodeposited nickel–sulfide films as competent hydrogen evolution catalysts in neutral water. *J. Mater. Chem. A* **2**(45), 19407 (2014).
38. C. Tang, Z.H. Pu, Q. Liu, A.M. Asiri, Y.L. Luo, and X.P. Sun: Ni₃S₂ nanosheets array supported on Ni foam: A novel efficient three-dimensional hydrogen-evolving electrocatalyst in both neutral and basic solutions. *Int. J. Hydrogen Energy* **40**(14), 4727 (2015).
39. X.D. Yan, L.H. Tian, M. He, and X.B. Chen: Three-dimensional crystalline/amorphous Co/Co₃O₄ core/shell nanosheets as efficient electrocatalysts for the hydrogen evolution reaction. *Nano Lett.* **15**(9), 6015 (2015).
40. X. Yan, K. Li, L. Lyu, F. Song, J. He, D.M. Niu, L. Liu, X.L. Hu, and X.B. Chen: From water oxidation to reduction: Transformation from Ni_xCo_{3–x}O₄ nanowires to NiCo/NiCoO_x heterostructures. *ACS Appl. Mater. Interfaces* **8**(5), 3208 (2016).
41. Z.S. Wu, W.C. Ren, L. Wen, L.B. Gao, J.P. Zhao, Z.P. Chen, G.M. Zhou, F. Li, and H.M. Cheng: Graphene anchored with Co₃O₄ nanoparticles as anode of lithium ion batteries with enhanced reversible capacity and cyclic performance. *ACS Nano* **4**(6), 3187 (2010).
42. X. Huang, Z.Y. Zeng, Z.X. Fan, J.Q. Liu, and H. Zhang: Graphene-based electrodes. *Adv. Mater.* **24**(45), 5979 (2012).
43. D. Merki, S. Fierro, H. Vrubel, and X.L. Hu: Amorphous molybdenum sulfide films as catalysts for electrochemical hydrogen production in water. *Chem. Sci.* **2**(7), 1262 (2011).
44. J.L. Lv, H. Miura, M. Yang, and T.X. Liang: Synthesis of Ni₃S₂ nanotube arrays on nickel foam by catalysis of thermal reduced graphene for hydrogen evolution reaction. *Appl. Surf. Sci.* **399**, 769 (2017).
45. X. Yan, L. Tian, and X. Chen: Crystalline/amorphous Ni/NiO core/shell nanosheets as highly active electrocatalysts for hydrogen evolution reaction. *J. Power Sources* **300**, 336 (2015).
46. Y.Q. Teng, H.L. Zhao, Z.J. Zhang, Z.L. Li, Q. Xia, Y. Zhang, L.N. Zhao, X.F. Du, Z.H. Du, P.P. Lv, and K. Świerczek: MoS₂ nanosheets vertically grown on graphene sheets for lithium-ion battery anodes. *ACS Nano* **10**(9), 8526 (2016).
47. G. Zhou, D.W. Wang, L.C. Yin, N. Li, F. Li, and H.M. Cheng: Oxygen bridges between NiO nanosheets and graphene for improvement of lithium storage. *ACS Nano* **6**(4), 3214 (2012).
48. V-D. Dao, N.T.Q. Hoa, L.L. Larina, J-K. Lee, and H-S. Choi: Graphene–platinum nanohybrid as a robust and low-cost counter electrode for dye-sensitized solar cells. *Nanoscale* **5**, 12237 (2013).
49. H.Y. Jin, J. Wang, D.F. Su, Z.Z. Wei, Z.F. Pang, and Y. Wang: *In situ* cobalt–cobalt oxide/N-doped carbon hybrids as superior bifunctional electrocatalysts for hydrogen and oxygen evolution. *J. Am. Chem. Soc.* **137**(7), 2688 (2015).

Supplementary Material

To view supplementary material for this article, please visit <https://doi.org/10.1557/jmr.2017.270>.